Pergamon

Cement and Concrete Research 31 (2001) 1821–1830

CEMENT AND CONCRETE RESEARCH

# A neutron diffraction study of ice and water within a hardened cement paste during freeze–thaw

Ian P. Swainson[a,*], Erland M. Schulson[b]

[a]*Neutron Program for Materials Research, National Research Council of Canada, Chalk River Laboratories, Station 8, Chalk River, Ontario, Canada K0J 1P0*

[b]*Thayer School of Engineering, Dartmouth College, Hanover, NH 03755-8000, USA*

Received 3 January 2001; accepted 13 August 2001

**Abstract**

A 1-month-old, saturated rod of hardened Portland cement paste with w/c = 0.40 was formed with, and stored under, heavy water. This rod was studied undergoing two freeze–thaw cycles over the range 227–297 K, using neutron diffraction, at slow rates of heating and cooling. Neutron diffraction gives a direct and independent quantification of the amount of ice and liquid water in the pore system of hardened cement paste as a function of temperature. The amount of ice that formed was totally reproducible over two freeze–thaw cycles, implying negligible changes to the pore size distribution and geometry. An analysis of some of the factors that may contribute to the freeze–thaw hysteresis is given. There is significant broadening of the diffraction peaks of the ice, which corresponds to a small correlation length of crystalline order in the ice. Water was observed to be "irreversibly" expelled during the first freeze, above ca. 250 K.


*Keywords:* Neutron diffraction; Pore size distribution; Crystal size; Crystal structure; Freezing/thawing

## 1. Introduction

Hardened Portland cement paste (HCP) is a material that is porous over many length scales. Freezing is known to occur in the mesopores ($2 \leq d$ (nm) $\leq (50)$. Here we examine the behaviour of water-saturated material during two slow freeze–thaw cycles. We have previously investigated a sample of composition w/c = 0.36 during a single freeze–thaw cycle over 227–297 K [1], and found it to contain hexagonal ice, and that there was more ice on warming than on cooling at any temperature. Here we show it is possible to create a simultaneous relative measure of ice *and* water content inside the pore system of an HCP. Also, we find an expulsion of water from the bulk sample on freezing, and show that the freeze–thaw hysteresis in ice content is totally reproducible over the two cycles. It was noted in Ref. [1] that the observed hysteresis in ice content cannot be explained using only simple spherical and cylindrical pores, and standard thermoporometry. Here we extend the analysis by examining other factors that may contribute to the broad form of the hysteresis.

The breadth of the ice "Bragg" peaks is used to calculate an average coherence size for the ice crystals that form inside the pore system. The possible implications of the broadening for certain models of freezing inside the pores of HCP are discussed.

Several neutron techniques have been used to study cements in the past, including diffraction studies of ice [1,2], small angle scattering (SANS) measurements of microstructure with time [3,4], quasielastic neutron scattering (QNS) measurements of hydration reactions over time [5,6], and diffraction studies of matrix components [7,8]. Neutron applications in this field have recently been reviewed in Ref. [9]. The advantage of using neutrons for this work lies in both their sensitivity to hydrogen (both stable isotopes are good scatterers with different characteristics) and the penetrating nature of the radiation that ensures that the scattering is representative of the bulk of a sample.

Throughout the discussion, we will use $D_2O$ as a general chemical symbol irrespective of its state, and we use "water," "ice," or "vapour" where specific reference is needed.

* Corresponding author. Tel.: +1-613-584-8811x3995; fax: +1-613-584-4040.

*E-mail address*: ian.swainson@nrc.ca (I.P. Swainson).

0008-8846/01/$ – see front matter 
PII: S0008-8846(01)00704-9

## 2. Method

The material used in this study was prepared from Type II Portland cement and heavy water. The mass ratio of water to cement was 0.40. Heavy water ($D_2O$) was used instead of light water to reduce incoherent scattering. Cylindrical specimens (5 mm diameter × 50 mm) were cast in a Plexiglas mould, allowed to harden for about 3 days, ejected, and then submerged under lime-saturated heavy water for 1 month at room temperature. Subsequently, they were encapsulated in vanadium tubes whose diameter was such that they just fit inside. The encapsulation was done in helium so that the initial atmosphere around the sample was helium gas. Indium wire was used to try to seal the tube. The samples were then irradiated with monochromatic thermal neutrons of wavelength 0.13286 nm (using a Si {531} reflection). Care was taken to ensure that the specimens were centered in the beam. The beam size was adjusted so that temperature sensors and the stainless steel cap were not irradiated. A small helium-filled gap between the top of the cement sample and the stainless steel cap existed. The specimens were cooled from room temperature (298 K) to 227 K in increments of 5 K and then warmed to 298 K within a liquid helium cryostat. Care was also taken not to thermally quench the samples below the bulk freezing point on initially placing them into the cryostat. This is because rapid freezing can damage the cement paste. Further details on the specifics of the cryostat and temperature control are provided in Ref. [1].

Data were obtained in terms of scattered intensity vs. diffraction angle 2θ (where θ is the Bragg angle), using the C2 spectrometer of Chalk River Laboratories NRU (Charles River, Ontario, Canada) reactor. The angle 2θ ranged from 9° to 89° for each run at each temperature. The counting time at each temperature was ca. 45 min, and the equilibration time at each temperature between 15 and 20 min. The total length of time used for these two cycles exceeded 4 days. The time taken between exceeding the bulk freezing point, $T_m$, during the first thaw and reducing the temperature below $T_m$ during the second freeze was around 15 h.

## 3. The nature of the ice: "Bragg" peaks and peak broadening

Fig. 1 shows diffraction patterns of the HCP as a function of temperature taken during the first freeze. The new ice "Bragg" peaks are immediately apparent in the region

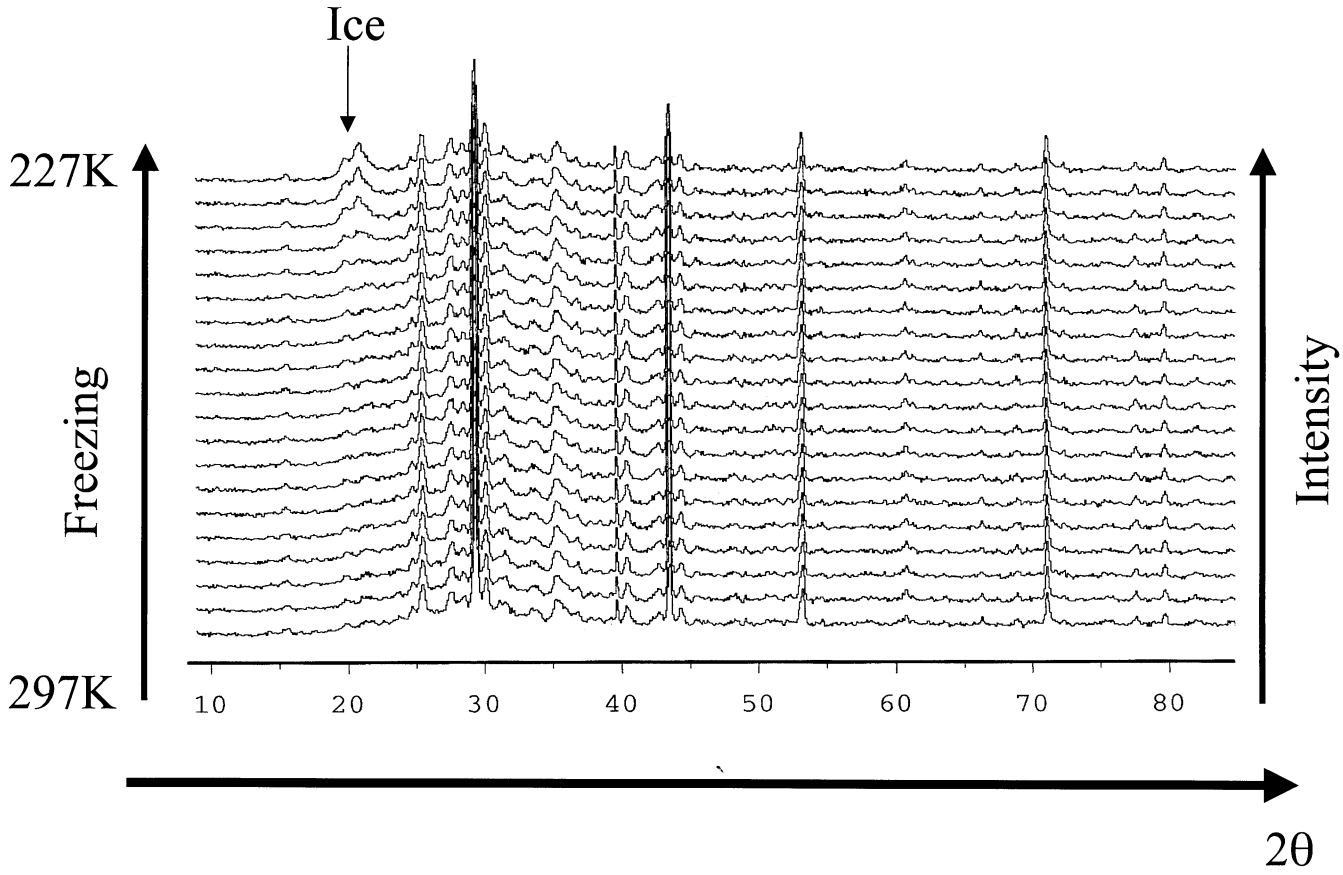


Fig. 1. Neutron diffraction patterns from w/c = 0.40 cement as a function of temperature. The new "Bragg" peaks due to ice are clearly visible at low temperatures.

ca. 19–22° 2θ. There are at least two peaks representative of ice in this region, ruling out the possibility that only Ic ice is present [1]. These two peaks correspond to 100 and 002 of the Ih structure.

These "Bragg" peaks are significantly broader than neighbouring peaks, which represent scattering from the bulk of the cement paste matrix — an observation also reported in Ref. [2]. Such broadening indicates a correlation length in the ice of a smaller dimension that the "coherence" or "correlation" length of neutron diffraction, which is often quoted as around 80 nm, as with X-rays. Excellent reviews of size and strain broadening in diffraction are available in Ref. [10]. One could interpret the broadening in several ways.

• As indicative of a glass. This was suggested for ice forming in 30 Å pores of silica glass [11]. However, this seems an unlikely explanation for the ice peaks seen in the pores of cement on the basis of the data presented here and in previous reports [1,2]. In Ref. [2], several orders of reflections were seen, ruling out any possibility of being a glass. In Ref. [1] and in the data presented here, two closely spaced peaks are resolved, also suggesting that it is crystalline in nature.

• As microstrain broadening. This occurs when there is a distribution of strain states within the coherence length of the radiation. One might argue that this could be the case for ice in pores, but in general, microstrain broadening increases strongly with increasing orders of reflection, with the lowest-order reflections remaining fairly sharp. This was not reported in Ref. [2], although they observed several orders of reflection.

• As domain size ("particle size") broadening, reflecting the limited size of the ice crystallites inside the pore structure. This appears to be the most likely explanation, as the ice forms in restricted pores. Fang et al. [2] estimated the broadening in their diffraction lines of ice Ic as due to crystallites of dimensions between 5 and 10 nm. By fitting peaks to the observed 100 and 002 lines of ice Ih at 227 K, we obtain estimates of the average coherent length scale of ca. 8.5 nm, in good agreement with Ref. [2]. This number represents an order of magnitude calculation, as it must average scattering from all the crystallites formed down to 227 K.

Fang et al. [2] demonstrate the existence of cubic ice Ic inside their HCP samples, and Ic has been observed in porous silica glass [11,12]. Ic is usually considered to be a metastable state in the bulk, so its apparent stability in certain porous samples is highly interesting. However, metastable states are frequently observed in porous systems [13]. It may be that cooling rates are important, and that Ic is a kinetic phase, easier to nucleate than Ih. Cooling rate information appears to be absent in these reports of Ic in pores [11,12,14]. If there is little free energy difference between the two phases and a large activation energy penalty, then at low temperatures, once nucleated, Ic may be very slow to transform to Ih. As a solid approaches its melting point, the mean square displacements rise, making the transformation to the equilibrium phase easier. Evidence for this comes from observations that Ic in silica pores transforms to Ih just before melting [14]. Various reports of Ih and Ic occurring in porous systems are discussed in Ref. [13].

## 4. Ice and water signals

Fitting Gaussian or Voigt functions to the ice peaks in Fig. 1 could lead to ignoring the background underlying these peaks, which contains very useful information. Instead, we perform a simple integration of all the counts over an area of the diffraction pattern. A plot of the integrated intensity of the region of the ice peaks as a function of temperature over the two cycles is shown in Fig. 2 over the interval 18–24.4° 2θ ($Q$=1.478–2.000 Å$^{-1}$), where $Q=2\pi/d$. It is apparent that there is a significant difference between the two freeze cycles at small depression temperatures. In fact, there is less total scattering in this range after the first freeze, as witnessed by the lower counts for temperatures greater than the bulk freezing temperature, $T_m$=276.8 K. Since there is no ice for $T>T_m$, this implies that there must be a fall in the background underlying the ice peaks. A correction is therefore required to account for the drop in the level underneath the ice peaks that would cause a systematic understatement of ice content with temperature. Despite this difference, it is apparent that the total scattering agrees over both thawing curves, and also the freezing curves, below ca. 250 K.

Fig. 3 shows a difference plot, created by subtracting the diffraction pattern at 297 K (before the first freeze) from that at 227 K (at the coldest point of the first freeze). As expected, there is a positive differential representing the new ice peaks 100 and 002, and one other weak peak visible due to ice at ca. 34.3° 2θ, which corresponds to 110 of the Ih cell. However, there is also a very broad depression underlying

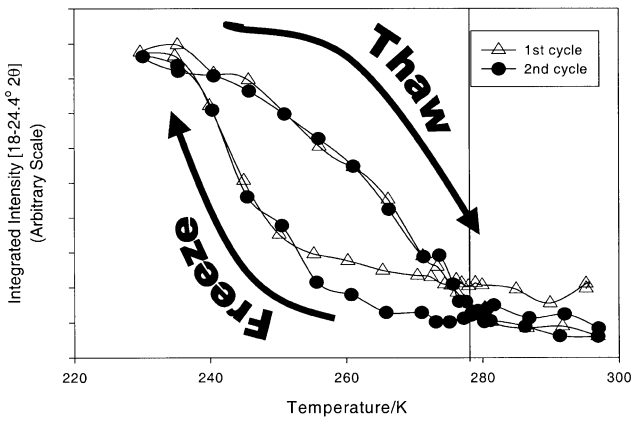


Fig. 2. Integrated intensity over the range 18–24.4° 2θ. This function is not reproducible over the two cycles.

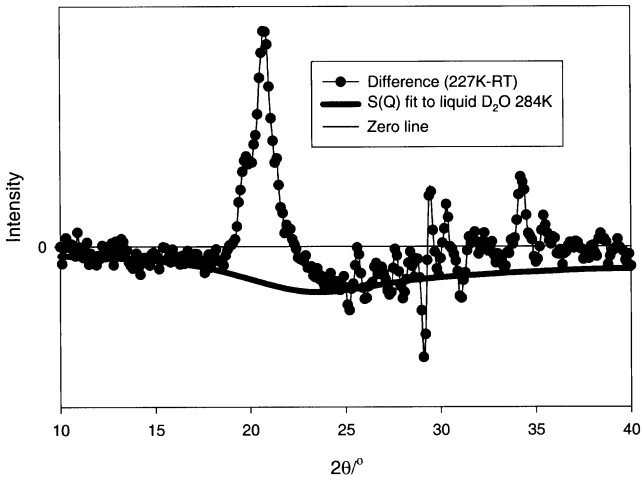


Fig. 3. Difference plot of the neutron diffraction patterns at 227 K and room temperature. The positive difference is the new ice "Bragg" peaks and the depression underlying this is fitted to the $S(Q)$ of liquid $D_2O$.

this. This depression is due to the removal of liquid water, mostly to form ice. This is demonstrated in Fig. 3 by the fit of $S(Q)$, the normalized structure factor of liquid $D_2O$ to this background. The data for the liquid $D_2O$ scattering are from Ref. [15] and are strictly valid only at 284 K, but it is clear that this is the explanation for the fall in the background. This implies that if care is taken, neutron diffraction is capable of simultaneously being an independent monitor of the proportions of both liquid water and solid ice inside the pore system of cement paste.

Fig. 3 also shows that the strong doublet representing the ice peaks is at a lower angle (larger $d$-spacing) than the maximum in the broad liquid scattering. The greater breadth of the scattering from the liquid phase and the different positions of the scattering maxima mean that it is relatively simple to separate ice and water scattering. This is done by performing another simple summation of the scattering over the range in which the change in the scattering pattern is due to the change in the proportion of liquid. The region of the diffraction pattern immediately beyond the ice peaks, 22.5–24.4° 2θ (1.8438–2.000 $Å^{-1}$), can therefore be used as an indicator of the water content of the pores during the freeze–thaw experiment. Fig. 4 shows the resulting water content over the two freeze–thaw cycles. In this figure, the normalization is such that the initial water content of the saturated sample is 0, and the water content at 227 K, corresponding to maximum ice content, is −1. This does not exclude the possibility of some unfrozen water still being present in the system.

We should carefully distinguish the measure presented in Fig. 4 from thermogravimetric analyses (TGA). TGA gives an absolute measure of water loss by evaporation from the pore system, since it measures changes in weight of a sample with changes in temperature. Fig. 4 is well described as a "water level meter," as it is a relative measure of losses of liquid due to both expulsion *and* removal to form ice.

There are two important things to notice about the water level during the freeze–thaw.

(i) Clearly, the amount of water that is present before the first freeze is greater than that after the first thaw. This implies loss of liquid water from the pore system, in agreement with previous TGA measurements and other observations [16].

(ii) Below 250 K during the second freeze–thaw cycle, the water level tracks that of the first freeze–thaw cycle. The implication is that the "permanent" expulsion of water takes place above 250 K. Below 250 K, the composite loss of water to form ice or from desorption or other expulsion losses is fully reversible.

It seems unlikely that significant quantities of liquid water could drain to the bottom of the tube and freeze, as we would record this contribution to the signal.

Note that there is a blip in Fig. 4 on the thawing leg of the first cycle at ca. 255 K. This represents a minor temperature excursion. This is reflected in some of the following figures that these data are used to construct (see below).

## 5. Thermodynamic driving forces for $D_2O$ migration

Expulsion is the external manifestation of migration processes of $D_2O$ inside the pore system. There are two broad classes of migration — those moving $D_2O$ towards freezing centres (including freezing pores, and the external, "bulk" environment), and those moving it away from freezing centres.

### 5.1. Migration towards freezing centres

On cooling, vapour pressure differences (e.g., Refs. [16–19]) between those pores with unfrozen liquid and those pores with ice inside them can cause migration from small pores to larger ones and to the exterior of the sample. This is because below $T_m$, the vapour pressure above a liquid is higher than that above a solid, giving a driving

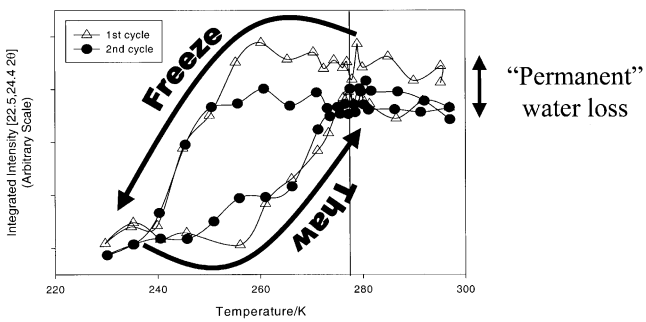


Fig. 4. Integrated intensity over the range 22.5–24.4° 2θ (arbitrary scale). This represents the change in scattering due to the loss of liquid $D_2O$. There is more water prior to the first freeze, than after the first thaw. Water is irreversibly lost during the early stages of freezing.

force for desorption and transport within the pore system. This is similar to the phenomenon of "cryopumping" in vacuum systems. The efficacy of vapour transport as a transport mechanism within pores has been questioned [20]. Litvan proposed that evaporation would occur until the meniscus acquires a negative curvature great enough to reduce the vapour pressure of water to that of ice. It has been shown [20] that this development of curvature can also be achieved by flow of water through the connected porosity and that this is orders of magnitude faster than vapour transport, especially in small pores. Everrett [21] also demonstrated a plausible thermodynamic driving force for liquid transport from smaller, unfrozen pores to freezing sites in porous solids, and that excess pressure builds up when a coarse pore is connected to a supply of water in a fine capillary.

### 5.2. Migration from freezing centres

This is caused by the large molar volume increase, $\Delta V^{\text{ice}}_{\text{water}}$, upon freezing, which is around 9% for bulk water. There are differences in the character of pore water and pure bulk water. These differences include smaller numbers of linear hydrogen bonds in pore water than in bulk water, which may explain the pore size-dependent latent heat of fusion [11]. In addition, in cement, there is a high degree of calcia saturation in the pore water. Despite this, Feldman [22] showed that the $\Delta V^{\text{ice}}_{\text{water}}$ observed for pore water freezing inside porous glass is very close to that of bulk water. A pore that is initially full must therefore either expand (possibly by fracturing the pore wall) or expel water out of the freezing pore into the neighboring pores. In a fully saturated network of pores, there will be no empty space for this extra volume. The pressure can either be relieved by expelling water from the sample if there is still a percolation path to the surface, or, if blocked by ice lenses, some part of the specimen must expand or fail to take up the volume. There is no preferred direction of travel from the freezing pore, other than that minimizing pressure.

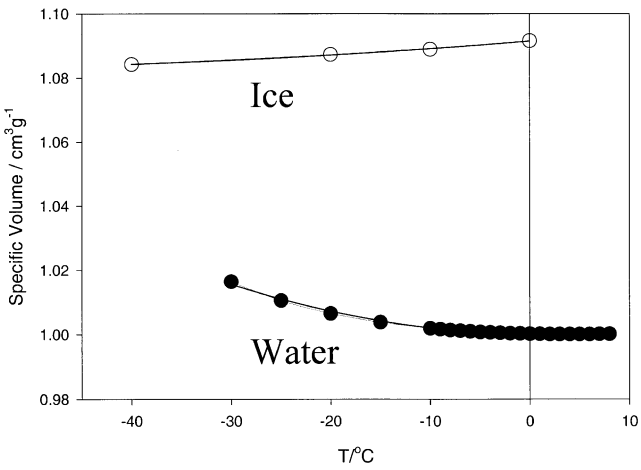


Fig. 5. Plot of the specific volume of supercooled light water and ice Ih as a function of temperature. Data are from H.D. Megaw, Nature 134 (1934) 900–901, and R.C. Weast (Ed.), CRC Handbook of Chemistry and Physics, 57th ed., CRC Press, 1976.

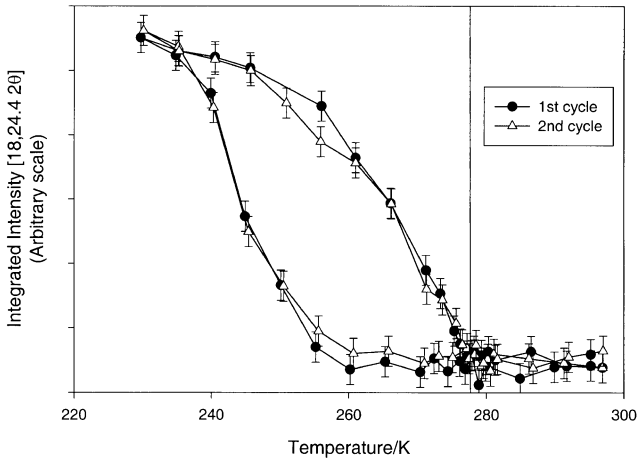


Fig. 6. Integrated intensity over the range 18–24.4° 2θ (arbitrary scale), corrected for the loss of water, using data from Fig. 4. This represents scattering only from solid $D_2O$, and is reproducible over the two cycles.

Fig. 5 shows the specific volume of bulk (supercooled, light) water and ice as a function of temperature. To the extent that bulk water can be used as a proxy for pore water, it is apparent that the $\Delta V^{\text{ice}}_{\text{water}}$ on freezing inside pores at $T < T_{\text{m}}$ may be slightly less than equilibrium freezing of bulk water, since water expands while ice contracts on cooling below $T_{\text{m}}$. Furthermore, the CSH matrix also contracts on cooling. Therefore, even if freezing did not occur, some water would have to be expelled from a saturated pore system.

## 6. Constructing independent ice and water monitors

It is possible to use the independent measure of the water level in Fig. 4 to correct the composite measure of "ice and water" in Fig. 2. A single parameter was used to scale the data from Fig. 4 to correct for the drop of background underneath the ice peaks in Fig. 2. Fig. 6 represents the resulting scattering from ice only. The most important feature to note from this is that it is totally reproducible over two cycles, within the error of the experiment. In order to avoid various biases introduced, we chose not to fit Gaussians to the ice peaks, which would avoid the "background problem." However, if one does so, a similar result ensues: the ice content is reproducible over the two cycles.

In Fig. 7, we have taken the mean ice content over the two cycles (for clarity) and added the water level from Fig. 2. The "permanent" expulsion of water takes place above 250 K during the first freeze. This coincides with the first appearance of ice inside the pore system. It would appear that $\Delta V^{\text{ice}}_{\text{water}}$ is likely to be correlated to this loss. Losses greater than three to four times that attributable to $\Delta V^{\text{ice}}_{\text{water}}$ have been reported before [16–19]. To within the precision

of the data in Fig. 7, it appears that approximately 23 ± 8.5% of the total water loss over the cycle is permanently ejected. There is appreciable error in this measure as it comes from integrating the broad water signal. We have to conclude that much of this leaves from near the surface of the sample as vapour and possibly escapes our sample can.

Of course, it could be argued that the permanent water loss could occur by cracking of the pore walls during freezing, and subsequent reaction of pore water with remnant cement clinker in the matrix. The matrix away from the pore walls is relatively unhydrated. This is evident from the difference in neutron diffraction patterns observed from HCP rods ground in air and under heavy water. In the former case, light water is absorbed by the HCP from the air, and the result is a large amount of incoherent neutron scattering. In the latter case, the diffraction pattern from the solid rod changes slightly due to additional hydration reactions [23]. One would expect to see either new weak peaks, indicative of the formation of new hydrous phases, or increase in the intensity of peaks representative of preexisting hydrous phases. Neither was observed in the diffraction patterns of the solid rods after freeze–thaw. Thus, this idea of additional hydration seems improbable. Instead, the water must have been ejected from the sample as concluded above.

## 7. Freeze–thaw hysteresis

Thermoporometry provides a good description of predicting freezing and thawing temperatures of many porous systems [24,25]. It was developed for single-phase materials, e.g., γ-alumina and $NiF_2$ [24]. The observed freezing and thawing behaviour in these materials could be described in terms a combination of pore size distributions of pure spheres ($f=1$) and of pure cylinders ($f=2$). It is easy to envisage a continuous variation between these endpoints by taking a sphere and extending one axis so that one gets an ellipsoid of revolution, becoming progressively more prolate and with less curvature, until it reaches a limit where it effectively becomes a cylinder. Thermoporometry [24,25] gives the following numerical relationships for water. For freezing:

$$\Delta T = \frac{64.67}{r-0.57}, \tag{1}$$

and for thawing

$$\Delta T = \frac{64.67 f^{-1}}{r-0.68}, \tag{2}$$

where the depression temperature $\Delta T = T - T_m$, $T$ is the temperature in Kelvin, $r$ the radius of the pore in nm, and $f$ the shape factor. We can refer to the radius that is characteristic of freezing at a given temperature $T$ in a pore of radius $r$ as $r_T$. For thawing, we can simplify Eq. (2) to:

$$\Delta T = \frac{64.67}{\Re-0.68}, \tag{3}$$

where

$$\Re = 0.68(1-f) + fr \tag{4}$$

and $\Re$ represents the radius of a spherical pore that would melt at this temperature. Effectively, pores of equal curvature melt at the same temperature.

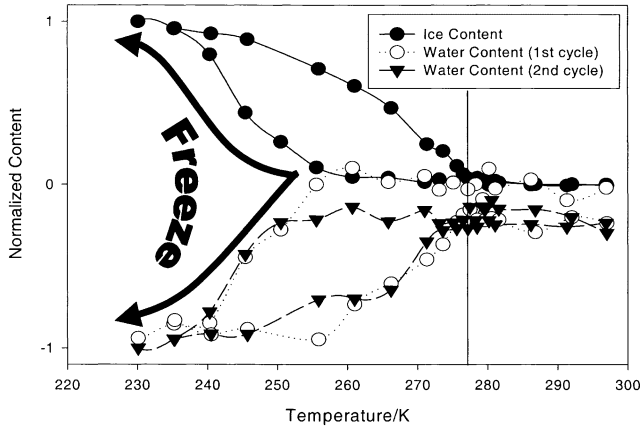


Fig. 7. Mean ice content and water content over the two freeze–thaw cycles.

### 7.1. Interpreting the freezing curve

The original papers on thermoporometry [24,25] were not specific about whether the freezing process in pores is a nucleation-dominated, or a growth-dominated, event. It is possible to interpret the equations in both ways.

(i) As *independent* pores that would spontaneously freeze throughout the sample via nucleation; i.e., at a given $T$, all the pores of $r_T$ would freeze at the same time.

(ii)As a percolating ice front that grows by travelling through the connected pore network [26]; i.e., as pores whose states (frozen/unfrozen) are *totally dependent* on the states of their neighbors. The interpretation of the radius in thermoporometry equations then becomes that of the breakthrough radius, $r_{BT}$, of the neck connecting a neighboring frozen pore to an unfrozen one.

In the latter case, the following equation is important:

$$\Delta T \approx \frac{2\gamma\cos\theta}{(r_{BT}-\delta)\Delta S}, \tag{5}$$

where γ is the ice–water interfacial energy, $\Delta S$ the entropy of fusion per volume of crystal, θ the contact angle between ice and the pore wall, and δ the thickness of unfrozen water between ice and pore wall, which may be temperature-dependent. This equation is essentially the same as that underlying the numerical relationship of Eq. (1) (see, e.g., Refs. [24,25]).

The rate of homogeneous nucleation inside pores is likely to be so slow that it would not occur on the time scale of typical thermoporometry experiments [28]. Heterogeneous nucleation could occur, but the temperature at which this occurs at an appreciable rate is dependent on the contact

angle, and bears no relation to radii of pores or necks [26]. Also, if pore walls were effective nucleating agents, with a contact angle less than 90°, then the propagating front would permeate through the entire network instantly [26]. Therefore, it seems that the only mechanism that can explain progressive freezing as a function of temperature is (ii); i.e., that of the gradually percolating ice front.

If this is the case, then it becomes rather difficult to get unique information from a freezing curve. Clearly, since pores are larger than their necks, for a given $T$, all pores that have one or more necks with radii $r \geq r_{BT}$ may freeze. This would imply that one could interpret the freezing curve as a cumulative distribution of the volume of ice frozen inside pores with $r > r_{BT}$ that is representative of all such pores in the network. However, whether they *will* freeze is highly dependent on the connectivity of the pore system. Since it appears that freezing is a gradual percolation of an ice front through the network, some pores satisfying the radius criterion for freezing will not freeze at the predicted temperature. Freezing requires the ice front to be able to reach them, and for those pores a long way from the ice front, it is likely that there will be many constrictions along the way that will retard the arrival of the ice front, and they will remain unfrozen until temperatures lower than that predicted from Eq. (5). The same problems apply to the interpretation of mercury penetration and nitrogen desorption techniques.

To illustrate the importance of connectivity, consider the schematic of part of a linear pore system (Fig. 8). One can see that the same fragment of pore system could generate completely different freezing curves, depending on which direction the ice front approaches from. If it approaches from the left, then the first pore will freeze, but further freezing will not occur until 253 K when the ice front will instantly percolate the remaining network. If the ice front approaches from the right, then most of the pores will freeze by 261 K, with the exception of the leftmost pore that will not freeze until 253 K. This would generate two different freezing curves from one system.

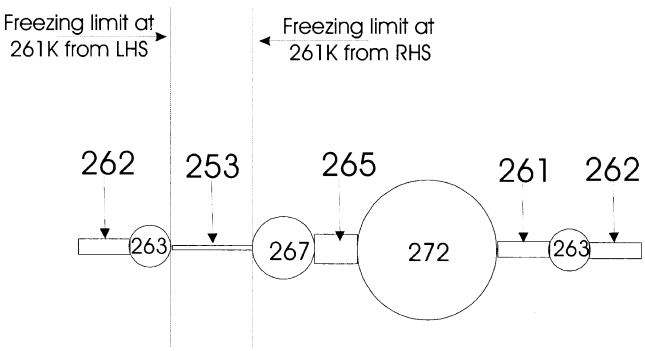


Fig. 8. Schematic of a linear pore system. This system has the same neck sizes at either side so the ice front can enter either side at 262 K, depending on the connectivity of this part of the pore system to the rest of the pore system, and the direction along which the ice front appears. Two different freezing curves are possible from this one system, depending on the direction of travel of the ice front.

Fig. 8 is an extreme case. There is only one pathway along which the ice front can migrate. In a real three-dimensional pore, network cross-linking will occur so that there are multiple paths through which the ice may move. While this reduces the "bottleneck" effect, it does not remove it entirely. The further away from the current ice front a pore is, the most likely it is that a "bottleneck" will prevent freezing from occurring. The freezing curve can probably never be interpreted as a unique "fingerprint" of the pore system of a given HCP.

A further complication to interpretation is that Eqs. (2)–(4) do not hold for such "ink bottle" pores, as there is no connection between the radius of the neck, which is the limiting factor determining freezing point depression of the pore, and the radius and shape factor of the interior of the pore, which govern melting.

That we do not observe appreciable ice formation until ca. 250 K could be interpreted in two ways.

(i) That a very thin layer of ice formed at the surface near $T_m$ which cannot make significant progress into the pore system until it penetrates bottlenecks with an $r_{BT} \approx 2.5$ nm.

(ii) That ice did not form at the surface near $T_m$ and the first ice nucleus formed somewhere inside the pore system as a random heterogeneous nucleation event. In the latter case, this nucleation temperature would contain no size information and we would have missed some information about large pore and neck connectivity.

A similar onset of freezing was seen in a w/c = 0.36 sample [1]. However, which mechanism is responsible cannot be answered from this dataset alone.

### 7.2. Interpreting the thawing curve

Unlike freezing, thawing is likely to occur in pores as a process independent of the state of the neighboring pores; i.e., all pores with a characteristic curvature, determined by $r$ and $f$, will thaw at the temperature given by Eq. (4). This would seem to make it simpler to interpret thawing and allow a unique interpretation of size and shape distributions possible, but this is not necessarily so.

In the initial thermoporometry papers [24,25], the issue of potential connectivity is ignored, and the 50% transformation point of the freezing and thawing curves was used to determine a characteristic mean value of $f$ for a material. For materials such as alumina, silica, Vycor, and titania, values between 1.25 and 1.94 were reported. Although systems with controlled pore sizes and shapes may yield information from Eqs. (2)–(4), this is probably not the case in HCP. HCP is porous over many length scales, and there is no control over pore shape, i.e., it is possible that $f$ may be better described as a broad shape distribution rather than a well-defined mean value. It is also possible that the shape distribution is itself pore size-dependent; e.g., smaller pores may be more likely to be nearly spherical and larger pores more likely to be nearly cylindrical. Without very detailed knowledge of this sort, it is

unlikely that one can deconvolute the size and shape distributions to obtain a unique interpretation of the thawing curve. In addition, attempts to use the freezing curve in conjunction with the thawing curve to determine characteristic values or distributions of $f$ are greatly complicated by the percolating nature of freezing and the nonpercolating nature of thawing.

There is one further process that may serve to broaden the freeze–thaw hysteresis, and this is the potential for redistribution of water within the pore system during freezing, especially if some pores are only initially partially filled. Considering the possible thermodynamic driving forces for mass transport, it is obvious that those driving forces for transport to freezing sites inherently drain $D_2O$ from smaller pores and feed them into larger, frozen pores. However, $\Delta V^{\text{ice}}_{\text{water}}$, the driving force for transport from freezing sites, may actually contribute to accumulation of ice in larger partially filled pores also. Although there is no inherent direction to the expulsion of water in this driving force, the only pores in which it will accumulate *and* freeze are larger, partially filled pores. Therefore, a freeze–thaw hysteresis has the potential to be widened by accumulation in such pores during an experiment: e.g., consider a large, nearly empty pore. On further cooling, water accumulates in this large pore to relieve the pressure due to $\Delta V^{\text{ice}}_{\text{water}}$ from freezing events elsewhere, and at some point, this initially empty pore will freeze. On thawing, there is now more $D_2O$ in large pores than there was when the experiment began, and this tends to move the thawing curve towards $T_m$.

As this sample was saturated prior to the start of the experiment, nominally all the pores were filled in the initial state. In nonsaturated pastes, one would expect this phenomenon to have a larger effect: this is because the large pores are the first to empty in low humidities and the last to fill at temperatures above freezing, and therefore will be likely to be only partly occupied at the onset of cooling.

### 7.3. Reproducibility of the freeze–thaw hysteresis

The reproducibility of the thawing curve implies that during the first freeze–thaw process, there was negligible change to the pore size and shape distributions through the sample. The reproducibility of the freezing curve implies that the size distributions of the pores and necks, and the pathways the freezing fronts took through the sample, were scarcely affected by the freeze–thaw process. Taken together, this implies that there was negligible fracturing of the pore walls during the first freeze. This apparent lack of pore wall cracking, and the lack of changes in diffraction patterns before and after freezing (Section 6), are strong evidence that the loss of water is not due to hydration reactions with unhydrated remnant clinker. The lack of pore wall cracking reinforces many earlier observations, made not at the mesoscopic level but at the level of specimen dimensions, that freeze–thaw damage is not solely caused by $\Delta V^{\text{ice}}_{\text{water}}$ (a point made by Ref. [19]) but is strongly affected by the cooling rates; e.g., Litvan [16] observed no permanent macroscopic distortion after a freeze–thaw cycle at a rate of 0.0417 °C/min in a w/c = 0.7 HCP.

### 7.4. Peak broadening of ice in the pores of HCP

The observation of peak broadening (Section 3) raises an interesting question for the ice front model. Broadening is not always observed when fluids are frozen inside porous structures. For instance, in water frozen inside gels [27], no broadening of X-rays peaks occurred, and this implies that the ice crystals that form in those particular structures are crystals that are continuous through many pores [28]; this has been taken as evidence of the existence of ice fronts in such systems. Broadening is also absent when freezing Ar, Kr, and $D_2$ in porous Vycor glass [29].

In Section 3, we showed that the most likely origin of the broadening was "particle size broadening," and that a correlation length scale of ca. 8.5 nm is consistent with our observations. One should also bear in mind that the correlation lengths one obtains from line widths do not necessarily correspond to physically distinct "crystallites." For instance, heavy Ic/Ih stacking faulting within a crystallite could also reduce the distance over which scattering is correlated within that crystallite by breaking it up into "domains." Whether the 8.5-nm length scale is generated by physically distinct crystallites, implying a lack of large-scale correlation of ice through the pore system, or due to heavy faulting within larger crystallites is unclear, but it does appear to differ from observations of ice and frozen fluids in other porous solids.

## 8. Comparison to w/c=0.36

The total intensity of the ice peaks in the w/c = 0.40 sample is approximately 2.2 times that of the w/c = 0.36 sample of Ref. [1] at 225 K. However, if the data from both samples are compared by scaling the signal to unity at 225 K, the shapes of the freeze–thaw hysteresis are very similar, implying similar distributions of pore shapes and sizes.

The total signal present in the region of the ice "Bragg" peaks is systematically lower in the w/c = 0.36 cement after the thaw than before the freeze. The drop is within the statistics of that experiment, as there was much less liquid water present in this drier cement. It was for this reason that it was not reported in Ref. [1], but it does appear to be consistent with the current observations.

## 9. Extension of measurements to lower temperatures

We performed a short measurement to examine what happens when a w/c = 0.40 HCP is cooled below ca. 230 K. This sample was from the same batch as that

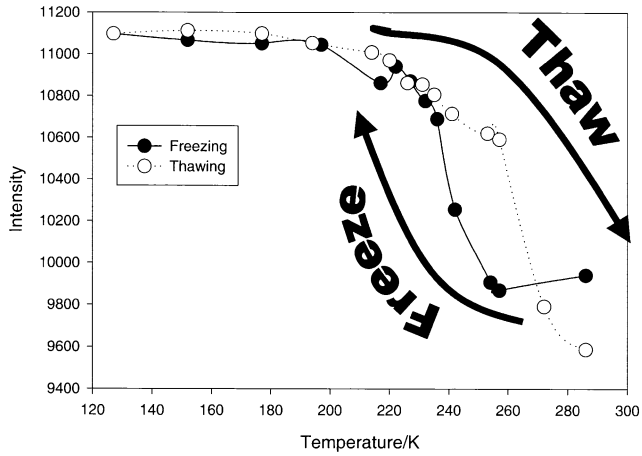


Fig. 9. Freeze–thaw curve over an extended temperature range. There is little new ice production below 220 K.

used in the main study, but was 8 months old during this run. A closed-cycle refrigerator was used for cooling and equilibration times were shorter than in the main experiment, but the aim was to see how much further the hysteresis extends down in temperature. Again, we saw two peaks indicative of the presence of Ih. Fig. 9 shows a plot uncorrected for water loss, but integrated over a restricted range of 19–22.5° 2θ, which minimizes the effect of water loss on the values. There is a small gain in ice content below 235 K, and the thawing curve appears to follow the freezing curve for approximately 100 K. For most of the region less than 235 K, the ice content has nearly plateaued. This small increase could be viewed as freezing in pores of very small dimensions (<1.6 nm), or temperature-dependent reduction of the liquid boundary layer between ice and the pore wall, the δ of Eq. (5).

## 10. Conclusions

Neutron diffraction data can provide an independent relative measure of ice and liquid water content in the pore system of HCP as a function of temperature.

Both the freezing and thawing curves prove very difficult to interpret on a mesoscopic basis. The thawing curve should be simpler to interpret due to the nonpercolating nature of thawing, which leaves every pore independent. Nevertheless, a lot of knowledge of size and shape distributions and their correlations would be required to provide a mesoscopic interpretation. Due to the percolating nature of freezing, at any temperature one is simultaneously measuring an inequality in neck and pore size distributions satisfying $r \geq r_{BT}$ and the connectivity of the pore system.

A "permanent" loss of water was observed during the first freeze of the HCP. The permanent ejection coincided with the first significant ice formation inside the pores at ca. 250 K. It appears that $\Delta V^{ice}_{water}$ cannot explain all the water loss from this sample. Vapour loss appears to be the most probable explanation. Below around 235 K, the ice content shows little change, and no hysteresis is evident.

The breadth of the observed "Bragg" peaks appears to be generated by scattering from ice correlated over length scales of only ca. 8.5 nm. This appears to differ from observations of ice in other porous solids.

The amount of ice observed is totally reproducible over two cycles at all temperatures during freezing and thawing, implying negligible change in the pore size and shape distributions.

## Acknowledgments

We wish to acknowledge Ron Donaberger of NRC for modification of the cryostat and development of the cell used in this study. The work of one of us (E.M.S.) was sponsored by the US Federal Highway Administration through USA-CRREL, contract no. DACA 89-97-K-0007.

## References

[1] E.M. Schulson, I.P. Swainson, T.M. Holden, C.J. Korhonen, Hexagonal ice in hardened cement, Cem. Concr. Res. 30 (2000) 191–196.
[2] M.P. Fang, P.E. Sokol, J.Y. Jehng, W.P. Halperin, Neutron diffraction study of cement, J. Porous Mater. 6 (1999) 95–99.
[3] F. Haussler, M. Hempel, H. Baumbach, Long-time monitoring of the microstructural change in hardening cement paste by SANS, Adv. Cem. Res. 9 (1997) 139–147.
[4] J.J. Thomas, H.M. Jennings, A.J. Allen, Determination of the neutron scattering contrast of hydrated Portland cement paste using $H_2O/D_2O$ exchange, Adv. Cem. Based Mater. 7 (1998) 119–122.
[5] R. Berliner, M. Popovici, K. Herwig, H.M. Jennings, J. Thomas, Neutron scattering studies of hydrating cement pastes, Physica B 241–243 (1998) 1237–1239.
[6] R. Berliner, M. Popovici, K.W. Herwig, H.M. Jennings, J.J. Thomas, Quasi-elastic neutron scattering study of the effect of water-to-cement ratio on the hydration kinetics of tricalcium silicate, Cem. Concr. Res. 28 (1998) 231–243.
[7] R. Berliner, C. Ball, P.B. West, Reply to the discussion of the paper neutron powder diffraction investigation of model cement compounds, Cem. Concr. Res. 28 (1998) 1833–1836.
[8] R. Berliner, in: M. Cohen, S. Mindess, J. Skalny (Eds.), Materials Science of Concrete: The Sidney Diamond Symposium, American Ceramic Society, Westerville, OH, 1998, pp. 127–141.
[9] R.A. Livingston, D.A. Neumann, A.J. Allen, S.A. FitzGerald, R. Berliner, Application of neutron scattering to Portland cement, Neutron News 11 (2000) 18–24.
[10] R. Snyder, J. Fiala, H.J. Bunge (Eds.), Defect and microstructure analysis by diffraction, IUCR Monographs of Crystallography, vol. 10, Oxford Univ. Press, Oxford, UK, 1999 (ISBN 0 19 850189 7 (hbk).
[11] T. Takamuku, M. Yamagami, H. Wakita, Y. Masuda, T. Yamaguchi, Thermal property, structure, and dynamics of supercooled water in porous silica by calorimetry, neutron scattering, and NMR relaxation, J. Phys. Chem. B 101 (1997) 5730–5739.

[12] M. Dunn, J.C. Dore, P. Chieux, Structural studies of ice formation in porous silicas by neutron diffraction, J. Cryst. Growth 92 (1998) 233–238.
[13] L.D. Geld, K.E. Gubbins, R. Radhakrishnan, M. Sliwinska-Bartowiak, Phase separation in confined systems, Rep. Prog. Phys. 62 (1999) 1573–1659.
[14] M.C. Belissent-Funel, J. Lal, L. Bosio, Structural study of water confined in porous glass by neutron scattering, J. Chem. Phys. 98 (1993) 4246–4252.
[15] M.C. Belissent-Funel, J. Teixeira, L. Bosio, Structure of high-density amorphous water: II. Neutron scattering study, J. Chem. Phys. 87 (1987) 2231–2235.
[16] G.G. Litvan, Phase transitions of adsorbates: IV. Mechanism of frost action in hardened cement paste, J. Am. Ceram. Soc. 55 (1972) 38–42.
[17] E.W. Sidebottom, G.G. Litvan, Phase transitions of adsorbates: II. Vapour pressure and extension isotherms of the porous–glass+water system below 0 °C, Trans. Faraday Soc. 67 (1971) 2726–2736.
[18] G.G. Litvan, Phase transitions of adsorbates: III. Heat effects and dimensional changes in nonequilibrium temperature cycles, J. Colloid Interface Sci. 38 (1972) 75–83.
[19] J.J. Beaudoin, C. Macinnis, The mechanism of frost damage in hardened cement paste, Cem. Concr. Res. 4 (1974) 139–147.
[20] G.W. Scherer, Measuring permeability of rigid materials by a beam-bending method: I. Theory, J. Am. Ceram. Soc. 83 (2000) 2231–2239.
[21] D.H. Everrett, The thermodynamics of frost damage to porous solids, Trans. Faraday Soc. 57 (1961) 1541–1555.
[22] R.F. Feldman, Length change–adsorption relations for the water–porous glass system to −40 °C, Can. J. Chem. 48 (1970) 287–297.
[23] E.M. Schulson, I.P. Swainson, T.M. Holden, Internal stress induced through thermal mismatch: calcium hydroxide versus calcium silicate hydrate. Cem. Concr. Res. 31 (2001) 1785–1791.
[24] M. Brun, A. Lallemand, J.-F. Quinson, C. Eyraud, A new method of the simultaneous determination of the size and shape of pores: the thermoporometry, Thermochim. Acta 21 (1977) 59–88.
[25] J.F. Quinson, M. Brun, Progress in thermoporomety, in: K.K. Unger, J. Rouquerol, K.S.W. Sing, H. Kral (Eds.), Characterisation of Porous Solids, Elsevier, Amsterdam, 1988, pp. 307–315.
[26] G.W. Scherer, Crystallization in pores, Cem. Concr. Res. 29 (1999) 1347–1358.
[27] W. Kuhn, R. Bloch, P. Moser, Das beim gefrieren von gelen entschende eis, Experientia 18 (1962) 197–212.
[28] G.W. Scherer, Freezing gels, J. Non-Cryst. Solids 155 (1993) 1–25.
[29] D.W. Brown, P.E. Sokol, S.N. Ehrlich, New disorder induced phase transitions of classical rare gases in porous Vycor glass, Phys. Rev. Lett. 81 (1998) 1019–1022.